Flowfield and flame structure during intermittent transitions into thermoacoustic oscillations in a swirl stabilized model gas turbine combustor

Efstathios Karlis*, Yannis Hardalupas† and Alexander M.K.P. Taylor‡
Imperial College London, London, UK, SW7 2AZ

Development of gas turbine combustors operating on the lean premixed mode has been hindered by the establishment of thermoacoustic instabilities that may prove challenging to the structural integrity of the engine. Transitions between a quiescent state of thermoacoustic operation towards an oscillatory one occur via a Hopf bifurcation, namely via the emergence of periodic oscillations amidst broadband fluctuations. Hopf bifurcations can be distinguished between supercritical and subcritical, with the later type introducing especially undesirable effects due the abrupt and intermittent nature of their demonstration. Subcritical Hopf bifurcations in a model swirl stabilized gas turbine combustor are investigated in the current work. The system is driven towards the intermittently unstable regime namely close to the subcritical Hopf bifurcation point via gradual hydrogen enrichment of close to blow-off methane mixtures, at a constant equivalence ratio of 0.55. High speed (3 kHz) particle image velocimetry (PIV) measurements were employed to capture the flowfield structure during the transition from the stable to the unstable state. Phase conditioned low speed (10 Hz) OH planar laser induced fluorescence (PLIF) measurements provided information with regards to the flame structure. The transition from the low amplitude state towards the high amplitude one is always preceded by a precessing motion of the inner recirculation zone (IRZ) that is followed by a complete collapse of the IRZ. The collapse is caused by a disturbance of high positive axial velocity, convected downstream by the mean flow acting as the triggering event of the subcritical Hopf bifurcation. The PIV measurements show that the mean and standard deviation of the spatial distribution of the turbulent intensity increase, thus the flame interacts with a greater range of length scales during the intermittent bursts. This is also exemplified by the PDFs of the curvature distribution of the flame front quantified via PLIF. The analysis shows that transitional flames are more wrinkled than their quiescent counterparts, as evidenced by the higher curvature standard deviations and the lower curvature kurtosis values.

I. Introduction

Thermoacoustic instabilities under lean operation in gas turbine burners hinder the development of lean premixed combustion mode of operation, thus limiting the potential to reduce NO_x emissions. They arise from a mutual amplification between the acoustic field in the combustor and the heat release rate field [1]. Oscillations in dynamic pressure and heat release rate can prove detrimental to the structural integrity of the combustor, hence they have attracted significant research attention. The oscillations occur in a self-excited manner and once triggered, they become coherent, with a fundamental frequency of oscillation and potentially its harmonics. The manifold of attraction of the dynamics in the phase space is termed limit cycle [2]. On adjusting specific operational parameters, the dynamics bifurcate from a fixed point solution, wherein dynamics are randomly fluctuating under the influence of broadband turbulence, into a limit cycle, wherein deterministic periodic high amplitude oscillations are dominant, via a Hopf bifurcation [3]. A Hopf bifurcation can be either supercritical or subcritical in nature [4]. In the former, the system is linearly unstable, namely minute disturbances grow exponentially and saturate at a high amplitude state. In the latter, the system is linearly stable, but nonlinearly unstable. This means that only disturbances of finite amplitude can lead the system towards a limit cycle. On adjusting specific operational parameters, such as the equivalence ratio in a lean premixed gas turbine, the system is driven through a range of dynamic regimes wherein both the high amplitude (limit cycle) and the low

*Research Postgraduate, Department of Mechanical Engineering, E-mail address: ek3215@ic.ac.uk
†Professor, Department of Mechanical Engineering, E-mail address: y.hardalupas@ic.ac.uk
‡Professor, Department of Mechanical Engineering, E-mail address: a.m.taylor@ic.ac.uk

amplitude (fixed point) states are stable solutions of the trajectory of the system [5]. A finite disturbance with amplitude that is smaller than but still close to a triggering threshold amplitude might be damped or briefly cause transition to a high amplitude periodic state [6]. This is where the superposition of turbulence, acting as broadband noise, in a gas turbine combustor flowfield becomes significant. Turbulence may lead the system to successively "jump" between the fixed point and the limit cycle solution, in a random and stochastic manner. The regime, wherein the combustor demonstrates epochs of unstable behaviour amidst quiescent operation, is termed intermittency [7]. Intermittency in gas turbine combustors is manifested in short bursts of high amplitude heat release rate and dynamic pressure. This is an especially challenging issue in the operation of gas turbine combustors, since subcritical Hopf bifurcations arise in a self-excited abrupt manner and cause the system to suddenly transition from a stable operational state to an unstable one. The limit cycle perpetuates if the Rayleigh criterion is satisfied [8]. That is when the heat release rate and the dynamic pressure signals oscillate in phase, namely their relative phase of oscillations is within the range 0^o to 90^o with maximum amplitude of oscillations when their difference approaches 0^o.

The Rayleigh criterion describes the conditions for the perpetuation of thermoacoustic oscillations, however it does not state the underlying reasons driving the dynamics in gas turbine combustors into the unstable state from a stable one [9]. The current paper studies the characteristics of the dynamic state, the flowfield and the flame in a model swirl stabilized combustor, while the system demonstrates intermittent thermoacoustic behaviour. Triggering in subcritical bifurcations is especially undesirable in gas turbine combustors, because bi-stability can cause abrupt and unpredictable jumps to high amplitude dynamic states amidst a quiescent background. In [10], the bifurcation parameter in the operation of a combustor was the equivalence ratio ϕ, at constant Re. Upon increasing ϕ, from the lean extinction limit, an unstable state was encountered at a given ϕ_1 which led to full blown limit cycle oscillations. On decreasing ϕ, from the unstable state towards leaner ratios, a ϕ_2, different than ϕ_1, was found to establish requiescence again. The reported region of hysterisis covered a broad range on the $Re - \phi$ operational map, where the low amplitude dynamic pressure spectra were reportedly broadband and the high amplitude spectra featured distinct peaks indicating periodicity. Intermittent behaviour in the hysterisis region was not reported, indicating that subcritical bifurcations may feature hysterisis but not necessarily intermittency. In [11], the bifurcation parameters in a swirl stabilized combustor were the ϕ and the preheat temperature. Both of those bifurcation parameters were associated with hysterisis effects. Upon increasing either parameter, the flame assumed an M-shaped flame from a V-shaped one, similar to the flame shape bifurcations presented by [12] in the same configuration. In [13], in a swirl stabilized combustor burning methane, the bulk velocity was adjusted while maintaining ϕ constant. The dynamics transitioned successively from a stable, to an intermittent state and then to a limit cycle state upon increasing the bulk velocity and demonstrated a wide hysterisis range before establishment of low amplitude oscillations. Intermittent bursts also preceded the demonstration of a full blown limit cycle in their dynamic pressure spectra. The locus of attraction in phase space, otherwise referred to as an attractor [14], of the dynamic pressure signal demonstrated an elliptical orbit, while the correlation dimension [15] of the time series was equal to unity indicating that there was only a single time scale dictating the dynamics, namely the acoustic eigenmode of their geometry. In [16], bi-stability was attributed to a mechanism of pressure drop/recovery sequence in a swirl stabilized model combustor. The latter mechanism was also encountered in [17], in a work on the same geometry. A swirl stabilized combustor was susceptible to demonstrating subcritical Hopf bifurcations upon adjusting any of the preheat temperature, the air mass flow rate or the fuel mass flow rate, all of which drove the dynamics in hysterisis regions. The transition did not occur in a self-excited manner, but the flame was rather briefly forced via acoustic pertrubation of high amplitude. The dynamics remained attracted towards the high amplitude limit cycle even after forcing ceased. The bifurcation of the dynamics came about with a bifurcation of the flame shapes, with the shortest flame associated with the limit cycle and the longest, lifted flames with the low amplitude fixed point. It was conjectured that the subcritical nature of the bifurcations was associated with a saturation in the amplitude of the heat release rate with respect to incident velocity petrubations. In contrast, in [4], non-linearity and saturation were observed between the phase of the dynamic pressure and heat release rate signals, while the gain remained linear. Furthermore, in the same work which employed ϕ as the bifurcation parameter, the PDFs of dynamic pressure values elaborated clearly the superposition of gaussian and bimodal distributions for the intermittent regime. In [18], subcritical transitions were observed in DLR's burner employing high speed optical diagnostics. While the definition of thermoacoustic phase in this work was ambiguous, since the dynamics were not coherent, it was reported that the process of transitioning featured penetration of the flame towards the centerbody in the limit cycle state and lift-off in the quiescent state. Even though not explicitly stated in that work, the OH-PLIF images during the transition revealed a precession motion of the flame root, possibly under the influence of the PVC, similar to the observations of [19]. This observation was substantiated in [20], wherein the combustor was brought to the bi-stable regime by means of adjusting the equivalence

ratio. Spectral proper orthogonal decomposition revealed growth rates of coherent structures. Low density drifts caused by temperature variations led to an increase of the PVC's initially negative growth rate which approached zero. A random turbulent event further increased the growth rate to positive values. Once the PVC was strongly established, the growth rate noticeably increased through a self-amplification process, which effectively led to a thermoacoustic limit cycle. A stagnation point established close to the inlet axial stations of the combustor within the recirculation zone extinguished the flame from the inlet and from then on the growth rate saturated until a lifted M-shaped flame was formed. During the limit cycle, periodically formed symmetric vortex rings suppressed the PVC, whose power gradually decreased. On decaying PVC power, the limit cycle dynamic pressure amplitude decayed as well, before requiescence. In a swirl stabilized combustor in [21], the equivalence ratio was enriched for a quiescent V-shaped flame, which bifurcated subcritically towards a thermoacoustically unstable M-shaped flame, through a flame which was intermittent between V and M shapes. The mechanism of intermittency in that configuration was associated with a Ka that was defined as the ratio of the mixture extinction strain rate to the bulk azimuthal strain rate in their flow. Upon exceeding a critical Ka, in the context that was defined, it was suggested that there was increased probability for a flame to intrude into the ORZ. When intrusion was achieved, the consumption of products in that region caused intermittent high amplitude bursts, which became increasingly more frequent and finally established the M-shaped flame.

The previous paragraph, reviewed transitional mechanisms of subcritical Hopf bifurcations in model gas turbine combustors. An initial investigation of the mechanism that is associated with the corresponding bifurcation in the current geometry has been conducted in [22]. This experimental work showed that upon increasing the extinction strain rate of methane mixtures by blending hydrogen in increasing molar concentrations, the system underwent through intermittency before transitioning into a limit cycle. Intermittent thermoacoustic bursts were only observed when the elongated flame was able to overcome enhanced flow imposed strain rate and thus propagate towards upstream axial sections and thus anchor close to the centerbody. This anchoring property is crucial since the region downstream of the centerbody has been associated, in the relevant literature, with the existence of an azimuthal wavemaker, responsible for the generation of helical disturbances. Under the effect of the interaction with the wavemaker and before an intermittent burst, it was shown that the flame precesses before the establishment of a full-blown limit cycle or before requiescence. We were able to capture this behaviour of the flame, by timely triggering high speed optical diagnostics, such as Particle Image Velocimetry and Chemiluminescent emission measurements using the permutation entropy [23] as a forewarning signal of transitioning into deterministic dynamics from low amplitude stochastic fluctuations. In the current paper, we further our analysis on the flowfield structure during time instances that precede the establishment of a limit cycle, as the system undergoes transition through intermittent bursts. The structure of the extended abstract is as follows. Section II presents the experimental configuration of the swirl stabilized gas turbine combustor. Section III, presents results of the analysis. Instances of the flowfield during a subcritical Hopf bifurcation are examined as described through PIV measurements and OH-PLIF measurements. Finally, Section IV summarizes the findings of this work.

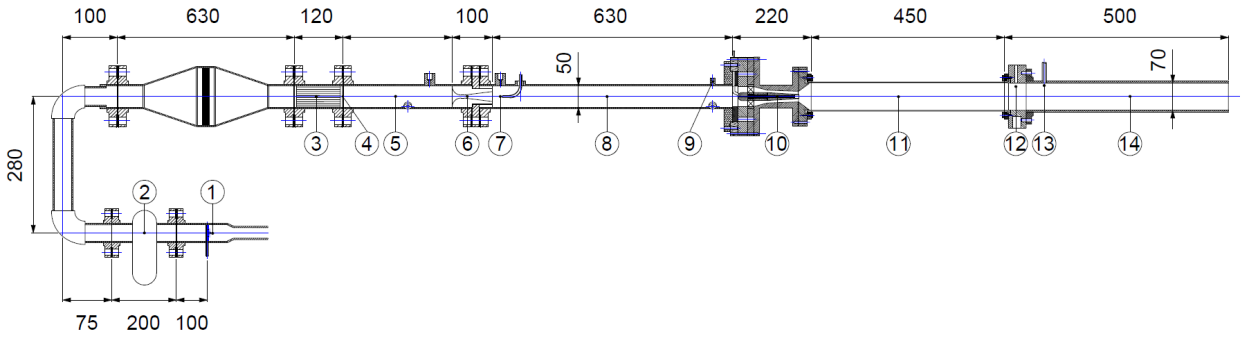


Fig. 1 2.1. Gas turbine combustor Figure 2.1: General overview of the experimental configuration. 1: upstream counterflow fuel injector for fully premixed measurements; 2: back- pressure regulator; 3: tube bundle flow straightener; 4: wire mesh gauge; 5: flow preconditioner; 6: critical Venturi nozzle; 7: seeding nozzle; 8: inlet plenum; 9: upstream dynamic pressure taping; 10: swirler; 11: fused silica combustor; 12: location of spark plug igniter; 13: Semi-infinite tube tapping; tapping; 14: exhaust. Dimensions in mm. Reproduced by [24].

II. Experimental configuration and instrumentation

The geometry of the experimental configuration is presented in Fig. 1 and a close up view of the model gas turbine swirl stabilized burner is depicted in Fig. 2. In the latter figure, in the squared smaller icon, a cross section of the centerbody at the point of injection is provided. A detailed description of the configuration can be found in [22] and [24]. Experiments were performed with hydrogen enriched methane. Air flowed from left to right in Fig. 1. The flow profile was conditioned by passing it through a tube bundle with a wire mesh gauge and through a flow straightener. A critical Venturi nozzle was installed downstream of the flow straightener to choke the air flow and provide a sonic boundary. Fuel was delivered at the centerbody of the swirler through ten equally spaced radial holes. Fuel and air are premixed at the injection point. The geometrical swirl number [25] based on the angle of the swirling blades was 0.7. Downstream of the swirler, the air-fuel mixture expanded through a diffuser. Optical access to the flame was granted by an optically accessible fused silica tube. At the end of the fused silica tube section, a tapping allowed the spark plug igniter to access the reactants. The transparent tube length was 450 mm and the duct diameter was 70 mm. A sample long exposure image of an elongated flame as viewed from the optically accessible window is depicted in Fig. 3(left). Downstream of the igniter a tapping assists the installation of a dynamic microphone to acquire data related to the acoustic field of the combustor. CH* chemiluminescent intensity measurements, acting as a proxy of heat release rate [26], were acquired using a photomultiplier that directed light intensity into a spectroscopic unit. Data were collected for 10 s at a sampling rate of 20 000 Hz in segments of 1024 samples for each experimental condition.

A. PIV measurements

The time dependent structure of the flow field was resolved through high speed Particle Image Velocimetry (PIV) experiments. Micron alumina particles were used to seed the flow, using a cy- clone seeder. The illumination source was an Edgewave Nd: YAG laser double pulsed at a rate of 3 kHz, emitting light at 532 nm. Pulse energies were 4 mJ/pulse and their relative time distance between each pair of illuminations was equal to dt =4 μs. The laser beam was formed by employing the optical configuration presented in Fig. 3 to create a profile with an approximately 1 mm waist thickness. The Mie scattering signal was captured with a Photron CMOS HighSpeed Star 2 equipped with a Nikkon lense (f /4.5, focal length 105mm) at a spatial resolution of 1024 ×992 pixels. The lens was fitted with a narrowband filter (Edmund Optics, 532nm ± 5nm) to suppress flame chemiluminescence from contaminating the image. Interrogation windows of 16 pixels by 16 pixels, overlapping by 75%, yielding a spatial resolution of 0.23 mm by 0.23 mm, were considered an optimum choice in the thesis. The vector yield using this size of interrogation window was 67081. The field of view, depicted in Fig. 3(right) was an axial slice of the combustor whose upstream edge was at the end of the diffuser at the inlet of the combustor and whose size was 60 mm by 60 mm. A schematic description of the optics and the laser beam path is presented in Fig. 4.

Figure 5 shows the flow field structure, as identified via high speed PIV and CH* chemiluminescent intensity measurements. The leftmost panel presents contours of axial velocity superimposed on mean streamlines, identified

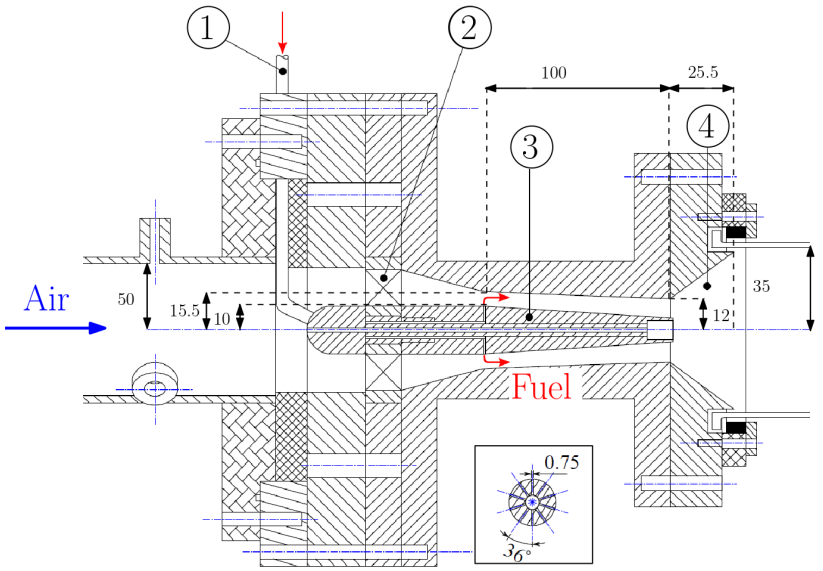


Fig. 2 Fuel injector and swirler. The following features are numbered: 1: Fuel supply; 2: Swirler blades; 3: Centerbody; 4: Diffuser. The air and fuel flow supplies are marked in blue and red respectively. The embedded sketch demonstrates a cross section of the centerbody at the axial station of the injection holes. Dimensions are in mm.

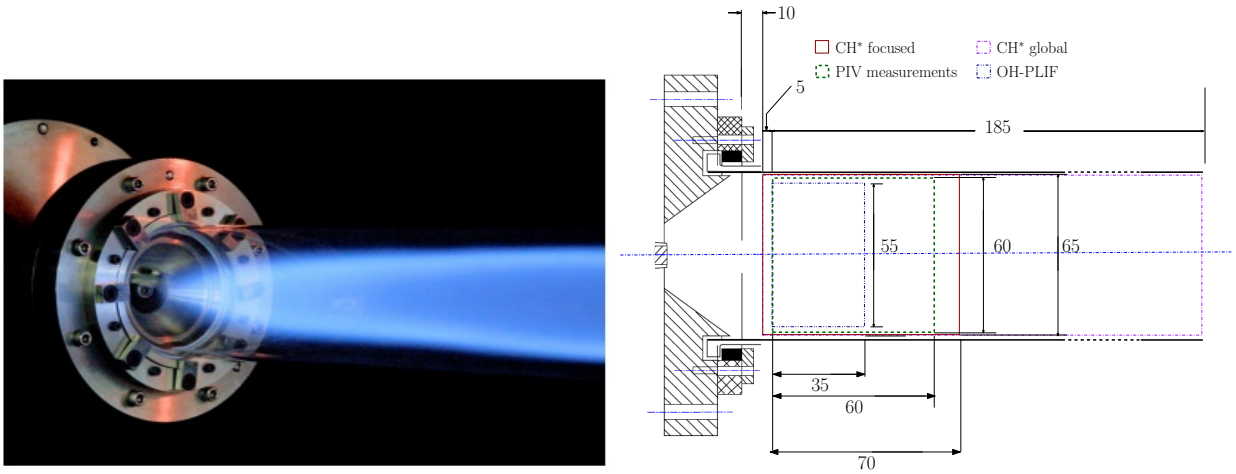


Fig. 3 Left: Long exposure image of a quiescent elongated flame, from [27]. Right: The field of views of the optical campaigns pursued in this work. The longitudinal dimension of the optically accessible part of the combustor is marked with continuous-dashed-continuous lines.

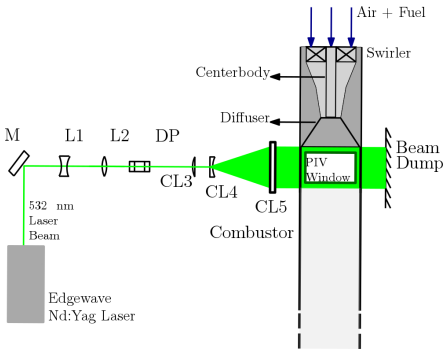


Fig. 4 A plan view of the optical configuration employed to generate the light sheet for the axial-radial field of view of the high speed PIV measurements. The HSS6 camera (not shown here) is placed below the combustor perpendicularly to the direction of the laser beam. M:Mirror, Spherical Singlet Lenses L1: -100mm, L2: 150mm, DP: Dove Prism, Cylindrical Lense CL3=400mm, CL4=-40mm, CL5=1000mm. Further details of the PIV campaign can be found in [24].

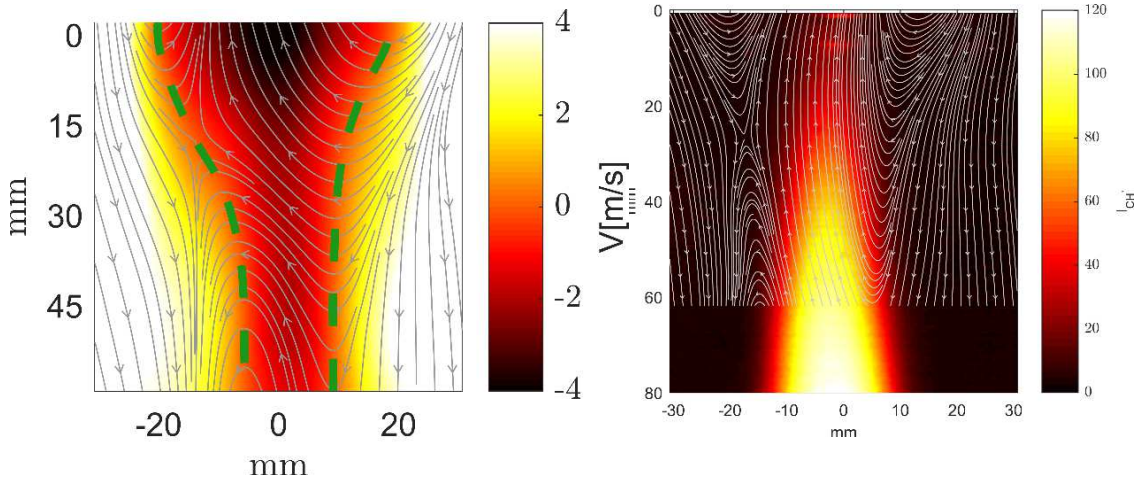


Fig. 5 (Left): Streamlines characterizing the mean flowfield while the combustor experiences quiescent operation. Streamlines are superimposed on contours of axial velocity. The green dashed line marks the iso-line of zero axial velocity (Right): Streamlines characterizing the mean flowfield superimposed on contours of CH* chemiluminescent emission intensity. The flow is from top to bottom. Reproduced by [22].

while the combustor demonstrated quiescent behaviour. The rightmost panel superimposes the location of heat release rate, as identified via CH* intensity high speed measurements on the mean flow field streamlines, when the flame was again quiescent. We identify a recirculation zone that extends along the whole length of the combustor, namely with no downstream stagnation point. The elongated flame anchors along the inner shear layers of the recirculation zone. The axial station marked as z=0 mm in Fig. 5 marks the start of the optically accessible part of the combustor, which coincides with the downstream end of the optically inaccessible diffuser.

B. PLIF measurements

The current Subsection describes the OH-PLIF excitation method and the optical setup. In the current experimental campaign, the electro-vibronic $Q_1(6)$ transition line was excited. Q transitions occur for ΔJ=0, with J being the rotational quantum number, [28]. The (1,0) band of the system $A^2\Sigma \rightarrow X^2\Pi$ transition, at 282.9 nm,was excited, collecting the fluorescent signal in the (0,0) and (1,1) bands around 308 nm and 314 nm [29]. The optical setup is depicted in Fig. 6. The second harmonic output at 532 nmof a Continuum Surellite III Nd:YAG was used as the pumping beam, with typical energy output around 0.450 J per pulse, into a Sirah Cobrah-Stretch dye laser. The dye of the resonator and the amplifier cells in the Sirah Cobrah-Stretch was Rohdamine 6G, dissolved in ethanol. The dye laser produced

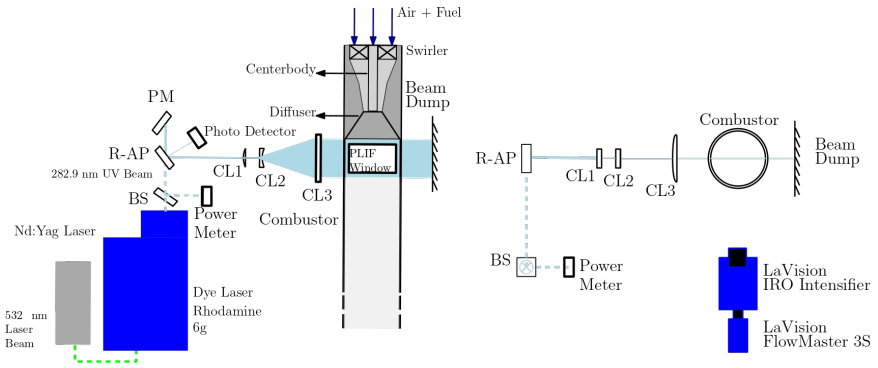


Fig. 6 Left: Plan view of the optical setup. Right: Elevation view of the optical setup. The dashed lines indicate laser beams below the height of the centreline of the combustor, whereas the continuous lines indicate leaser beams at the height of the same centreline. BS: Beamsplitter, PM:mirrors mounted on the periscope, R-AP: right-angle prism, CL1-UV=400 mm, CL2-UV=-25.4 mm, CL3-UV=250mm.

the laser beam that was used for the $Q_1(6)$ excitation. The tuning grating linewidth of the dye laser was $0.1 cm^{-1}$ at 570 nm. The dye laser energy per pulse was maximized by adjusting the Frequency Conversion Unit, achieving typical energy levels of 18 mJ per pulse. The height of the laser sheet was about 35mm and its thickness was about 1mm. The beam illuminated the region depicted in Fig. 6. The emitted fluorescence was captured by a LaVision FlowMaster 3S equipped with a LaVision IRO Intensifier. The intensifier was fitted with a UV-Nikkor Lens, (f/4.5,focal length 105 mm). An interference filter was fitted on the lens, in order to avoid capturing any laser light intensity. It was centred at 308.5 nm, had a maximum transmissivity of 25.5% and a full width half maximum (FWHM) of 18 nm. The lens was focused at the 35 mm x 55 mm region that is described in Fig. 6, while the resolution of the image was 876 pixels x 1376 pixels. The effective resolution of the acquisition was independently quantified, using a logarithmic bar-chart, as 5.0 lp/mm (where lp stands for line pairs). This was also considered the maximum resolvable curvature in the OH-PLIF experiments. The synchronization between the pump laser, the intensifier and the camera was achieved by using a LaVision Programmable Timing Unit (PTU) and a Quantum 9520 Series Pulse generator. The synchronization between the pump laser, the intensifier and the camera was achieved by using a LaVision Programmable Timing Unit (PTU) and a Quantum 9520 Series Pulse generator. The PTU's signal, instead of being directed to the flashlamp of the pump laser, was provided as a triggering pulse to a Quantum 9520 Series Pulse generator (temporal resolution 250 ps), because it was found that the characteristics of the step output provided by LaVision's PTU were not suitable for the triggering of the flashlamp of the pump laser. Crucially, care was taken to secure that the step profiles of the PTU and the Pulse generator were matched at the temporal resolution of the Pulse generator. The subsequent events of the acquisition were programmed based on time delays with respect to the PTU's reference triggering signal, but were delivered by the Pulse generator to the rest of the components.

C. Operational conditions

Experiments with blends of methane and hydrogen were conducted at a single Re=19000, at ϕ =0.55. The stoichiometric air to fuel ratio changed as a function of the relative molar concentration of the individual constituents. The purpose of this campaign was to adjust, independently of the equivalence ratio, the extinction strain rate of each premixture and then examine which dynamic state the combustor operated in. Combustion could not be sustained at χ_{H_2}=0 at this equivalence ratio. Upon increasing χ_{H_2} to 10% and 20%, the flame was stable and elongated. A further increase of χ_{H_2} up to 37.5% drove the combustor into an intermittent regime, while at χ_{H_2}=0.40 the flame demonstrated limit cycle Period-1 thermoacoustic oscillations. Hence, from the point where the flame would either blow out or not ignite at all at ϕ =0.55, H_2 enrichment at 40% established a thermoacoustically unstable flame at the same equivalence ratio. In the current work, focus will be placed on the structure of the flowfield during intermittent thermoacoustic bursts, namely the reported results correspond to cases MH055D, MH055E and MH055F as described in Table 1.

Table 1 Identification of the cases examined in the hydrogen enriched methane experimental campaign. The equivalence ratio was $\phi = 0.55$ at a constant Reynolds number $Re = 19000$. The table presents the molar fraction χ of the H_2 diluent, the dynamic state of the combustor, the numerically calculated extinction strain rate k_{ext}, the adiabatic flame temperature T_{ad}, the laminar flame speed $s_{l,0}$ and the Le of each mixture.

Case ID	$\chi : H_2$	ϕ	Dynamics	T_{ad}	k_{ext} [1/s]	$s_{l,0}$ [m/s]	Le_χ
MH055D	0.30	0.55	Intermittent	1587	1127	0.103	0.784
MH055E	0.35	0.55	Intermittent	1590	1250	0.106	0.748
MH055F	0.375	0.55	Intermittent	1592	1350	0.110	0.731

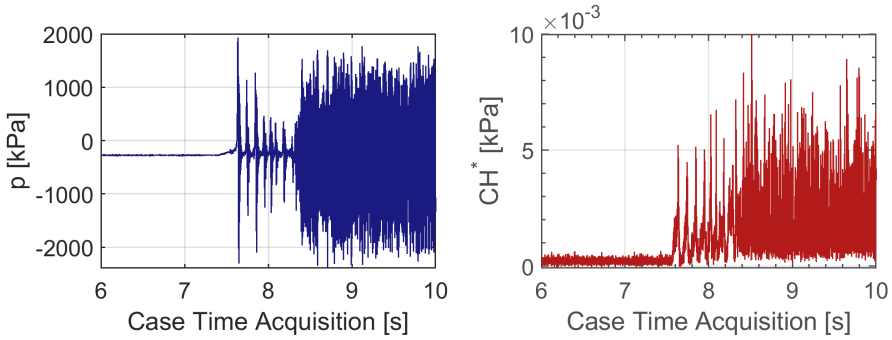


Fig. 7 Case MH055D: Time series of dynamic pressure (left) and heat release rate, measured by CH* chemiluminescent intensity (right). Three thermoacoustic conditions, namely low amplitude fluctuations (from the start until about 7.6 s), intermittent fluctuations (from 7.6 s until 8.6 s) and high amplitude oscillations (from 8.6 s onwards) can be identified.

III. Results and discussion

Figure 7 shows an instance of the experimentally acquired time series, while the combustor demonstrated intermittency. The operational conditions of this instance correspond to condition MH055D. The left panel shows the dynamic pressure signal, while the right panel shows the CH^* intensity signal from the photomultiplier. The phenomenon was demonstrated in a self-excited manner, while all operational parameters, such as air and fuel flow rates were kept constant at their nominal values. No forcing was introduced. We can observe three states of dynamic behaviour. From the start of the acquisition up until approximately 7.6s, the dynamics were quiescent with small amplitude turbulent fluctuations. From 7.6s until 8.5s, the dynamics demonstrated high amplitude intermittent bursts, a typical characteristic of subcritical bifurcations. From 8.5s onwards, the dynamics were fully unstable and demonstrated high amplitude heat release rate and dynamic pressure oscillations, being attracted towards a limit cycle.

Since the dynamics are non-ergodic, it is worth examining the FFT spectra corresponding to the distinct dynamic states. The intermittent states feature low amplitude dynamics, with a distinct peak at 20 Hz and a maximum amplitude equal to 130 dBa. The dynamics, post the Hopf bifurcation and the establishment of the limit cycle, feature a distinct peak at 160 Hz with an amplitude of 150 dBa. The mode corresponding to this frequency is the first quarter-wave acoustic mode, if the upstream duct boundary condition is modelled as $u'=0$ (imposed by the critical Venturi nozzle) and the downstream boundary condition is considered as $p'=0$ (at the exit of the combustor), as has been identified in [24]. The bifurcation is also reflected on the PDFs of the dynamic pressure signal. The PDFs of the dynamic pressure signal for the intermittent dynamics are symmetric about the 0 Pa value and feature a central mode with high kurtosis. Side modes of smaller probability at higher amplitudes can be observed as well. The side modes become dominant during the limit cycles state, with the PDF assuming a bimodal shape.

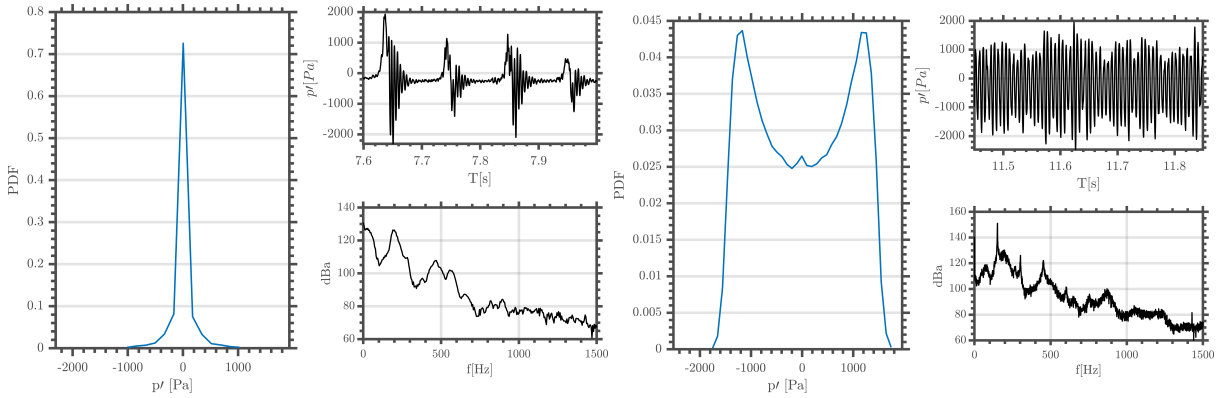


Fig. 8 Case MH055D: The leftmost set of panels corresponds to the intermittent stages of the time series depicted in Fig. 7, whereas the right set of panels corresponds to the limit cycle dynamics succeeding the intermittent bursts. Leftmost panel: the PDF of the dynamic pressure. Top rightmost panel: a magnified portion of the time series marked with a red square in Fig. 7. Bottom rightmost panel: the global FFT spectra acquired from the whole duration of the time.

A. Flowfield structure during thermoacoustic bursts

This section presents instantaneous flowfields during three stages of the first intermittent transition, namely at early signs of transitional behaviour, at the time of maximum dynamic pressure and finally at an event of requiescence. The segment of the signal that we examine corresponds to the first burst occurring between 7.63s and 7.68s in reference to Fig. 7. The presented flowfield snapshots that follow have been POD filtered, in order to make flowfield topologies and the underlying coherent structures discernible. Hence, the original snapshots have been reconstructed by using the 50 POD modes with the highest eigenvalues.

Fig. 9 provides instantaneous images of the flowfield at the early stages of an intermittent transition, shortly after the permutation entropy signal triggered the PIV acquisition. The bottom panel shows the dynamic pressure signal, with red circles marking the time when each presented flowfield snapshot was acquired. The bottom panel confirms that low amplitude pressure fluctuations are encountered at these times. Nevertheless, the signal demonstrates early signs of periodicity. Therefore, images are reported during a single period of the low amplitude signal, which resolve the temporal behaviour of the flowfield using eight snapshots. A helical structure can be identified that is wrapped around the shear layers of the recirculation zone, which forces the recirculation zone to a small precessing motion. At the same time, as the dynamic pressure signal assumes decreasing values during the single period event, the radial extent of the recirculation zone increases, while its axial extent decreases to the point that a downstream stagnation point is formed, within the PIV field of view. On increasing values of dynamic pressure during the single cycle event, the radial extent of the recirculation zone is decreasing again and the recirculation zone tends to assume an open-ended structure again (not shown on this set of flowfield snapshots). Figure 10 presents the temporal evolution of the flowfield that leads to the first high pressure intermittent oscillation. A disturbance of high amplitude positive axial velocity emanates from the inlet and is convected downstream by the mean flow. While the disturbance reaches further downstream axial stations, the axial extent of the recirculation zone decreases. The reason being that the axial disturbance accelerates the flow along in streamwise direction, hence reducing the swirl number. At the same time the recirculation zone precesses around the geometrical centreline of the combustor demonstrating greater azimuthal deflection than at the time of the case presented in Fig. 9. The dynamics return to quiescence briefly after the first intermittent burst. The respective temporal evolution of the flowfield behaviour is presented in Figure 11. This demonstrates the establishment of quiescent operation, which is associated with dissipating rates of azimuthal precession and decreasing amplitudes of axial velocity.

Precession around the geometrical axis of symmetry of the combustor is typically encountered in swirling flowfields and has been associated with the establishment of the Precessing Vortex Core (PVC) [30, 31]. The PVC is a helical coherent vortical structure that lies around the shear layers of the recirculation zone. It has been shown to affect the limit cycle dynamics of gas turbine combustors [32, 33], but it has not been associated before with the instigation of intermittent thermoacoustically oscillating dynamics. We assess that a PVC is present in the intermittent dynamics of the underlying flowfield in our geometry. Fig. 12 presents the first 6 POD modes of the flowfield, while Fig. 13 shows the corresponding Fourier spectra of the temporal coefficients of each POD mode. The Fourier spectra reveal

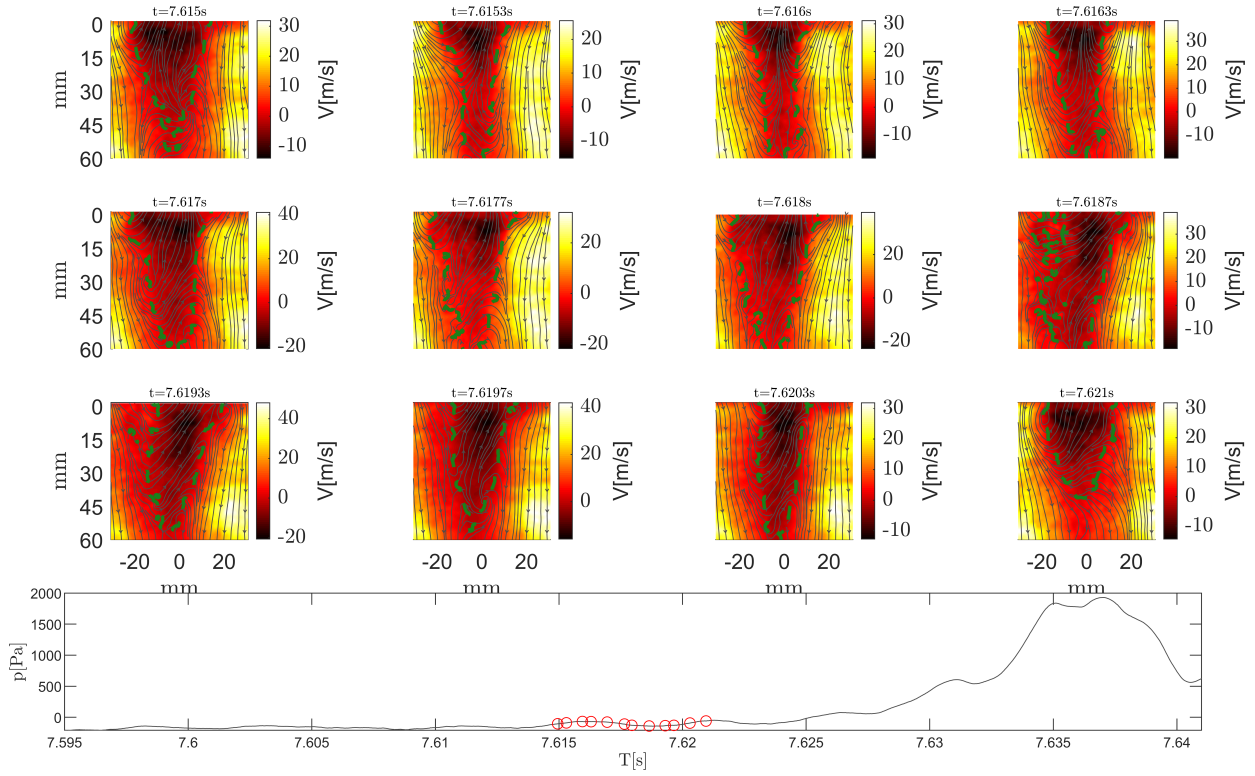


Fig. 9 Instantaneous time resolved flowfield during the early stages of the intermittent transition. Streamlines are superimposed on contours of axial velocity. The red circles superimposed on the dynamic pressure signal at the bottom panel mark the successive times when each PIV snapshot was acquired.

a low frequency time scale at about 20 Hz for all POD modes, which coincides with the low frequency contribution identified in the heat release rate spectra of Fig. 8. This timescale is related to the temporal distance between successive intermittent bursts of heat release rate and dynamic pressure. Modes 3 and 4 feature high amplitude peaks at about 65 Hz, while modes 5 and 6 reveal an additional contribution at a harmonic, namely at 130 Hz. All modes describe vortical structures that emanate from the inlet with decreasing intensity of vorticity. The observed two distinct time scales are possibly associated with azimuthal vortical waves of different wavenumbers that comprise the PVC in this configuration.

The transitional flame structure presented in Fig. 9 suggests that the thermoacoustically transient flowfield is subject to helical disturbances causing a precessing motion of the recirculation zone. Such a mechanism is commensurate with the existence of a PVC. The establishment of the PVC is associated in [34] with asymmetries between the radially homologous points of the flowfield. Radially homologous points are located at the same axial station, have the same distance from the combustor centreline, but are located on different radial halves. An indication of the extent of the radial asymmetry of the flowfield can be provided by Eq. 1.

$$R_{asym} = \left(\sum_{z_i=1}^{z_i=M} \sum_{a=0}^{a=R/2} (V(-a,z_i) - V(+a,z_i))^2 + \sum_{z_i=1}^{z_i=M} \sum_{a=1}^{a=R/2} (U(-a,z_i) - U(+a,z_i))^2 \right)^{1/2} \quad (1)$$

where M stands for the number of axial stations in the PIV measurements.

In Fig. 14, the temporal evolution of R_{asym}, normalized over the standard deviation of this quantity during the same PIV measurement, is superimposed on the normalized dynamic pressure oscillations. It is observed that the helical disturbances are explicitly depicted on R_{asym}, with the radial asymmetries being promoted on transitioning towards thermoacoustic instability.

It is of interest then to examine the temporal evolution of flow quantities of significance, during the demonstration of intermittency. Figure 15 presents the temporal evolution of the mean and standard deviations of the radial v' and axial u' spatially averaged RMS turbulent fluctuations. The bottom row of the same figure describes the normalized dynamic

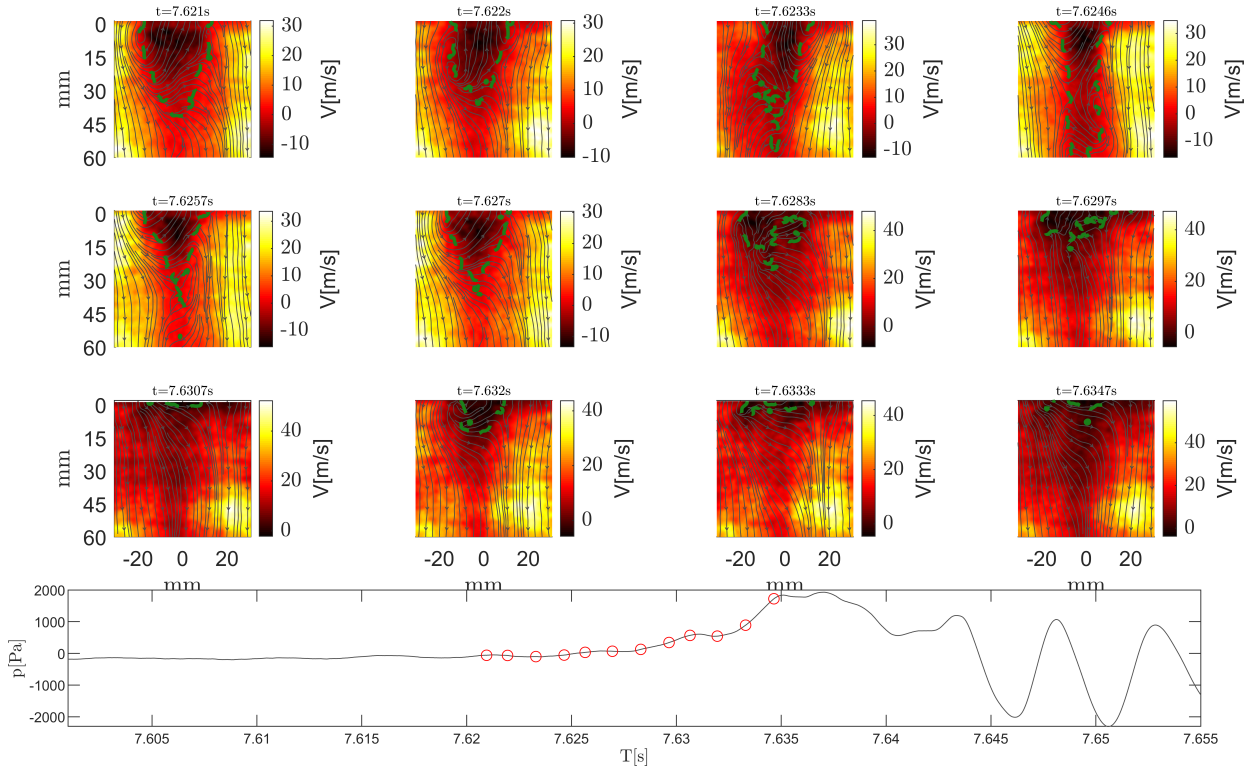


Fig. 10 Instantaneous time resolved flowfield during the time of the peak pressure of the intermittent transition to limit cycle oscillations. Streamlines are superimposed on contours of axial velocity. The red circles superimposed on the dynamic pressure signal at the bottom panel mark the successive times when each PIV snapshot was acquired.

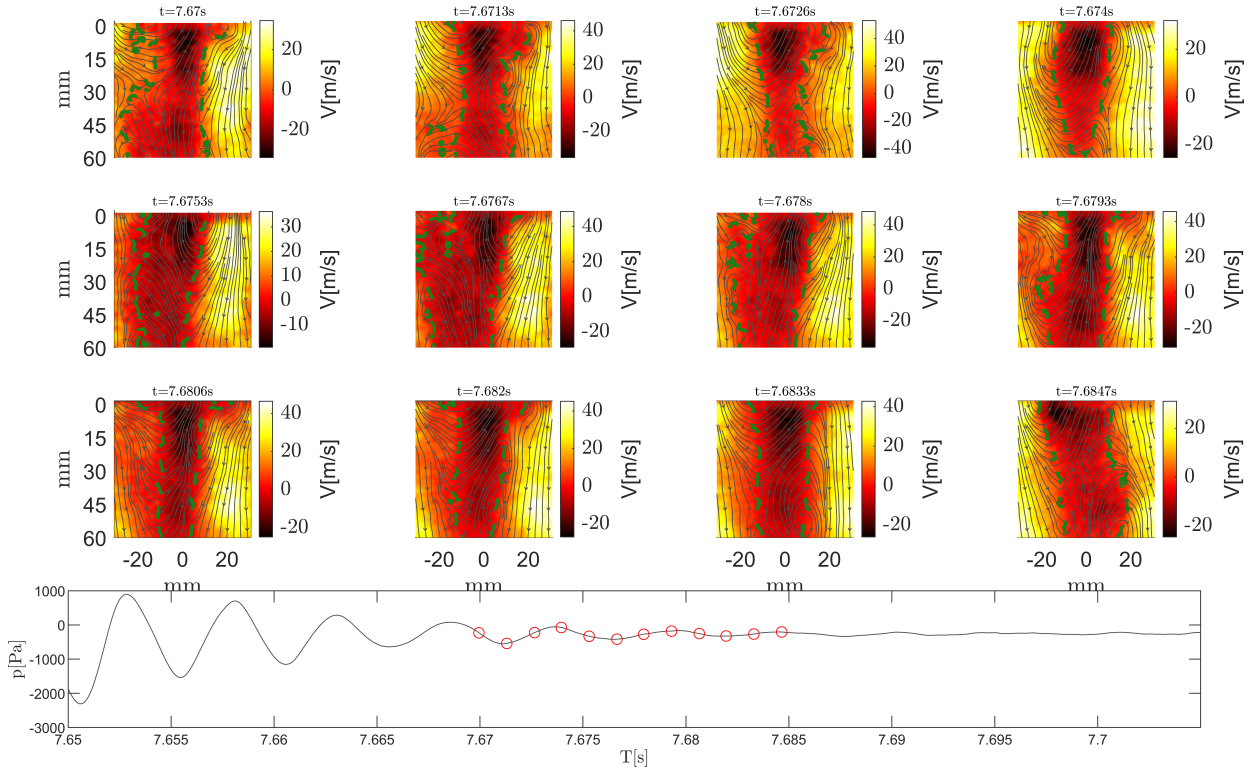


Fig. 11 Instantaneous time resolved flowfield during the time of the dissipating stage of the intermittent transition. The red circles superimposed on the dynamic pressure signal at the bottom panel mark the successive times when each PIV snapshot was acquired.

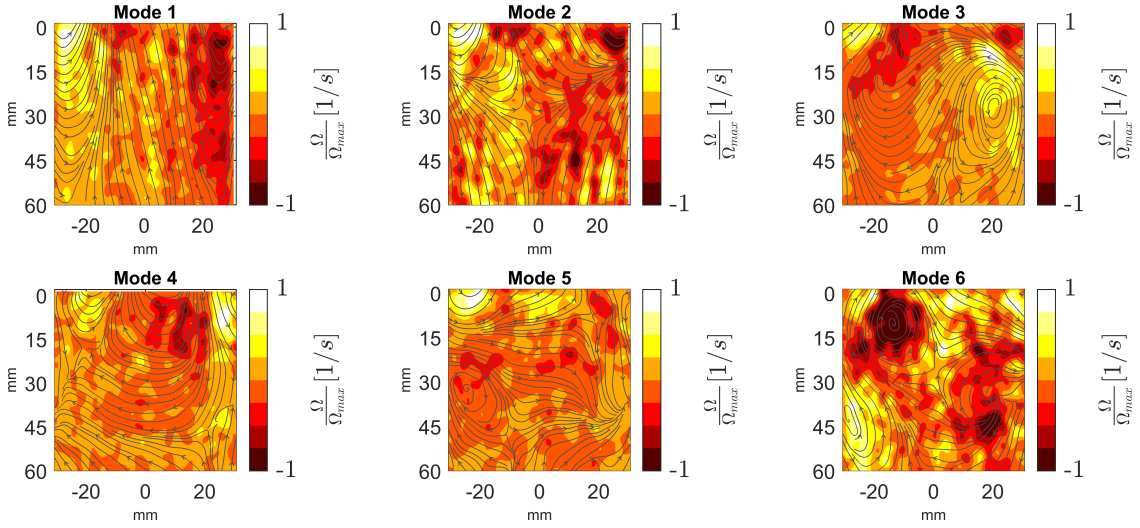


Fig. 12 POD modes of the flowfield while the combustor demonstrated intermittent behaviour. Streamlines are superimposed on contours of normalized vorticity. In reference to Figure 4 the modes have been calculated during the intermittent stages of the oscillations, namely from 7.6s until 8.5s.

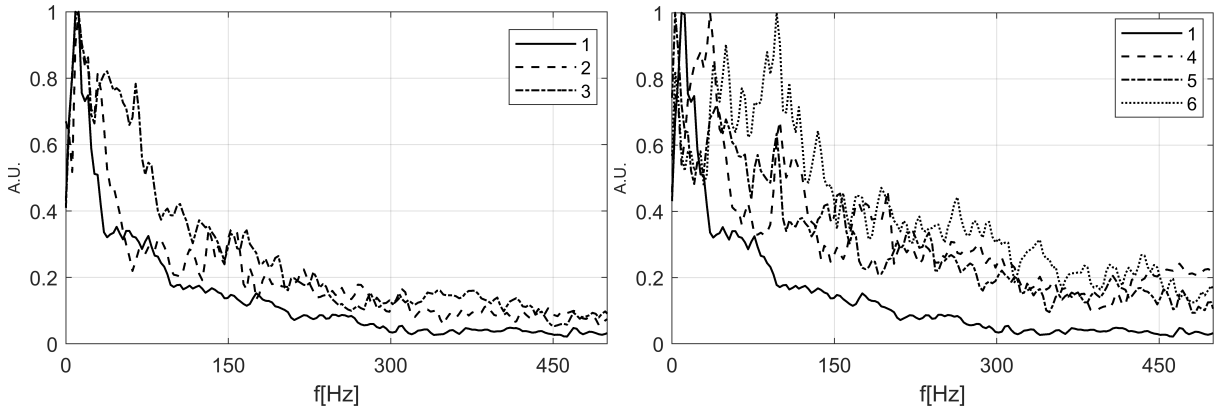


Fig. 13 Power spectra of the temporal coefficients of the first six POD eigenmodes, corresponding to the modes presented in Figure 12. In reference to Fig. 7 the temporal coefficients have been calculated during the intermittent stages of the oscillations, namely from 7.6s until 8.5s.

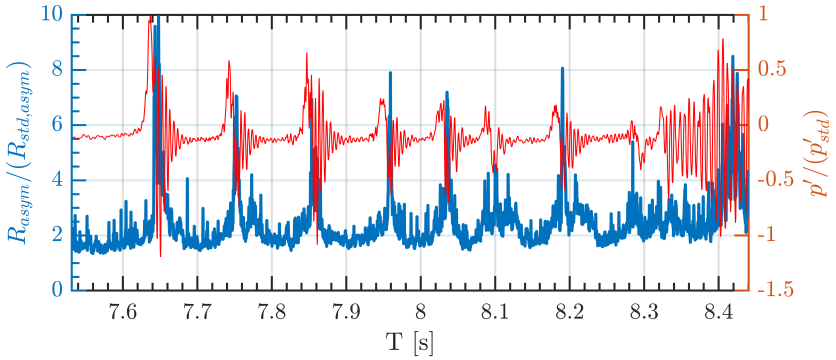


Fig. 14 The left axis indicates the intensity of radial asymmetry of the flowfield upon transitioning towards thermoacoustic instability, while the right axis indicates the corresponding dynamic pressure.

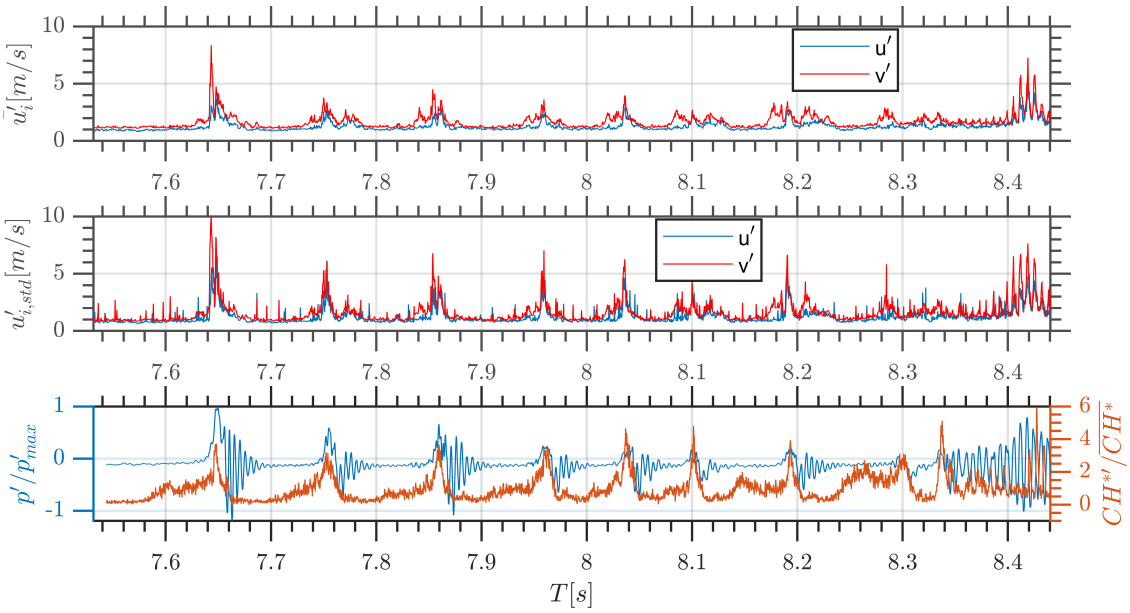


Fig. 15 A sample time series corresponding to a PIV acquisition during intermittent thermoacoustic instabilities. Top row: radial v′ and axial u′ spatially averaged RMS turbulent fluctuations. Middle row: spatial radial v′ and axial u′ standard deviation of the RMS turbulent fluctuations. Bottom row: normalized dynamic pressure (left axis) and normalized CH¤ intensity distribution (right axis).

pressure and heat release rate bursts during a PIV acquisition wherein multiple transitions were captured. It is observed that a thermoacoustic burst is associated with an up-to tenfold increase of the spatially averaged mean and standard deviation of the turbulent intensities. This indicates that during the transition towards self excited thermoacoustic oscillations, the mean intensity of the turbulent fluctuations increases. At the same time, the increased standard deviations imply that the flame interacts with a greater range of scales of eddies, on transitioning towards thermoacoustic instability. It is emphasized that this holds true at least within the range of scales that are resolvable by the PIV measurement. It can also be observed that the axial turbulent fluctuations are more sensitive to the sudden changes of the thermoacoustic state than the corresponding radial turbulent fluctuations.

B. Flame front curvature during transient events

The current Subsection reports on the flame front curvature characteristics for flames MH055D, MH055E and MH055F (see Table 1), whose thermoacoustic state is characterized as intermittent. In the current work, the flame front curvature was classified as positive if the flame was concave to the exhaust gases. An algorithm similar to the one presented in [35] was developed to extract the flame front from OH-PLIF images and then calculate the point wise curvature. Images were classified as corresponding to a quiescent, transient or limit cycle state, based on the following criteria. Initially, the envelope of the dynamic pressure signal was extracted by using the command *envelope* in Matlab. A sample result of a peak to peak envelope extraction process is provided in Fig. 16. Given the corresponding value of the dynamic pressure envelope, based on the temporal instance a PLIF image was extracted, an image was classified as quiescent, if the value of the envelope at the instance of the acquisition of a given image was lower than 300 Pa. If the value of the envelope was greater than 300 Pa, the image was a candidate of being classified as transient. A second criterion for the classification of an image as transient was to impose a requirement that the high amplitude burst would not last longer than 20 thermoacoustic cycles. If the latter criterion was not met, then the image was classified as corresponding to a limit cycle flame. In the sample envelope provided in Fig. 16, an OH-PLIF image acquired during the burst at 2.7 s would be classified as transient, while images acquired after 3.07 s would be classified as corresponding to a limit cycle flame.

It has already been documented in [22] that the quiescent flame is elongated, while the transitional flame is disturbed by helical structures and is occasionally advected closer to the walls of the combustor. Representative flame front curvatures corresponding to quiescent and transitional MH055E flames, are depicted in Figures 17a and 17b respectively.

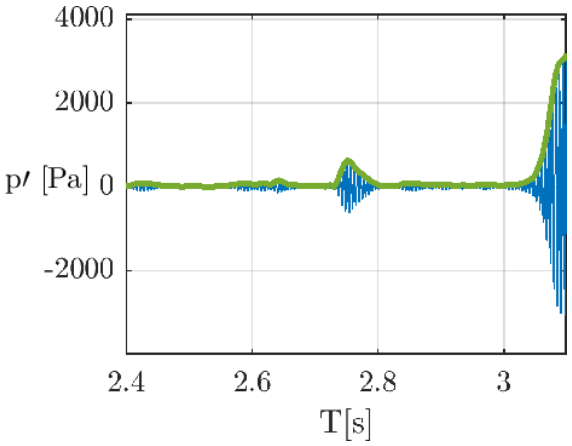
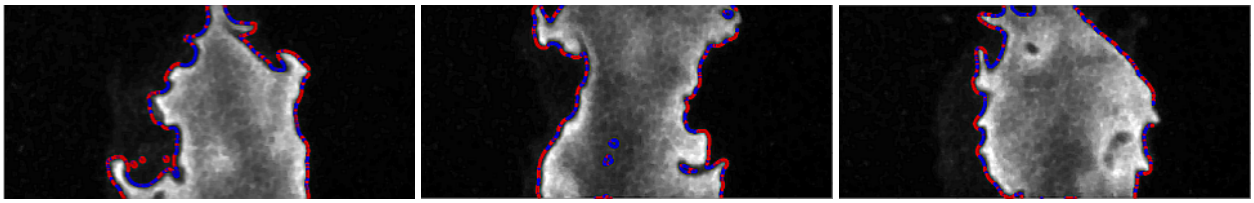
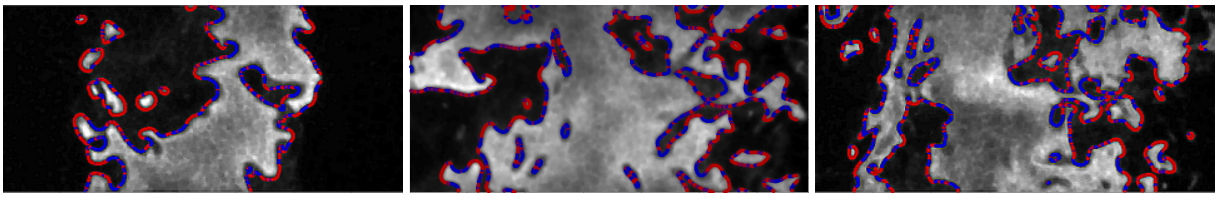


Fig. 16 A sample envelope (green thick line) of the dynamic pressure signal (blue line).

It can be observed that flames classified as transitional demonstrate longer flame fronts, anchor over greater radial extents within the combustor and may also demonstrate numerous flame holes and islands in comparison to quiescent flames. These initial observations motivated the currently reported statistical studies on the flame front curvature. Table 2 shows the statistical quantities of quiescent, transitional and limit cycle flames, demonstrating intermittency, while Figure 17 shows the respective histograms for each flame. The quiescent and transitional flames demonstrate positive means, in contrast to the global means of the limit cycle flame that assume negative values. The skewness values are again very close to zero, however the quiescent and transitional flames demonstrate positive skewness. This may be an indication of increased probabilities of formation of flame islands, associated with positive curvatures, however the deviation from zero is small. It is possible that the effect of the formation of flame islands on the flame front curvature is not strongly reflected on the skewness, due to the corresponding formation of flame holes. In addition, the standard deviations of the transient flames increase with respect to the quiescent flames, while the kurtosis values decrease. This is an indication of increased wrinkling of the transient flames, which is also demonstrated on the corresponding set of sub-figures 17b. The cause of the enhanced and abrupt "self-excited" wrinkling of the transitional flames is not clear, however it is corroborated by the findings presented in Fig. 15, regarding the temporal evolution of the turbulent intensities during the transition towards thermoacoustic instability. It is recalled that upon transitioning towards a high amplitude burst, the mean intensity of the turbulent fluctuations and their standard deviation increased. Arguably the turbulence due to the bulk Reynolds number of the flow does not play a role since the experimental conditions remain very close to the nominal ones throughout the acquisition. A possible explanation could be that the transient flames are associated with more intense burning than their quiescent counterparts, which is manifested via an increase of the flame surface through increased corrugation. This can also explain why the thermoacoustically unstable flames result being shorter than their quiescent counterparts. In addition, one would also need to consider that the interaction of the flame with turbulent coherent structures of the flowfield may also enhance the corrugation of the flame front. This interaction has been documented in [34], wherein it was argued that the interaction of a premixed flame with the PVC is responsible for the wrinkling of the flame front, over lengthscales, which were associated with the PVC. There is strong evidence hinting towards the crucial role of the PVC-flame interaction and the exhibition of intermittent thermoacoustic bursts. Finally, by considering that all of the limit cycle histograms feature decreased kurtosis values and increased standard deviations in comparison to the preceding transitional histograms, it may also be argued that the flame front curvature is one of the quantities that is involved in the mechanism of transition into thermoacoustic instabilities.



(a) OH-PLIF instances of thermoacoustically quiescent flames.

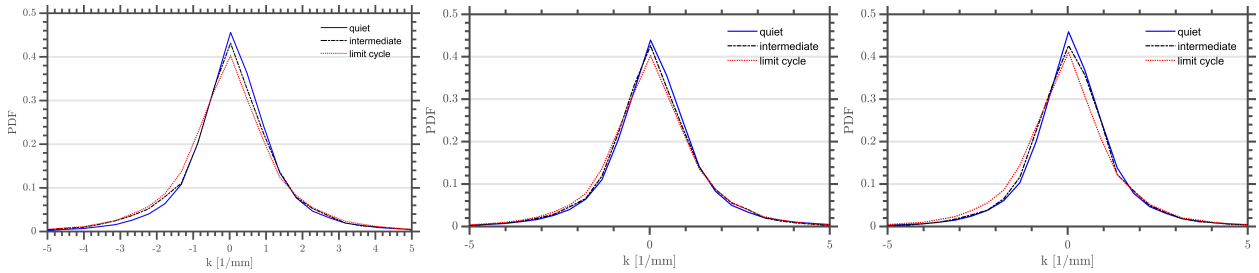


(b) OH-PLIF instances of thermoacoustically transient flames.

Fig. 17 OH-PLIF instances of an MH055E flame under quiescent and transient conditions.

Table 2 Global values of mean curvature $\overline{\kappa}$, standard deviation σ_k, skewness μ_3 and kurtosis μ_4 of flame front curvature, corresponding to the hydrogen enriched methane campaign.

Case ID/Thermoacoustic state	$\overline{\kappa}$	σ_κ	μ_3	μ_4
MH055D/Quiescent	0.115	1.108	0.091	5.045
MH055D/Transitional	0.167	1.128	0.095	4.794
MH055D/Limit cycle	-0.036	1.416	-0.036	4.472
MH055E/Quiescent	0.127	1.316	0.048	5.125
MH055E/Transitional	0.087	1.330	0.047	4.755
MH055E/Limit cycle	-0.048	1.408	-0.031	4.577
MH055F/Quiescent	0.122	1.264	0.027	5.344
MH055F/Transitional	0.089	1.296	0.028	5.120
MH055F/Limit cycle	-0.024	1.402	-0.013	4.598



(a) MH055D **(b) MH055E** **(c) MH055F**

Fig. 18 The flame front curvature histograms, corresponding to Table 2, conditioned with respect to the dynamic state (quiescent, transitional, limit cycle) for three cases of the hydrogen enriched methane campaign, which demonstrated intermittency.

IV. Conclusions

The paper focused on the flowfield and flame shape structure preceding an intermittent thermoacoustic burst. High speed PIV and phase conditioned OH-PLIF measurements were used to acquire insight with regards to the interaction of hydrogen enriched methane flames with its underlying flowfield during intermittent thermoacoustic bursts, while the system approached the point of a subcritical Hopf bifurcation. At a quiescent state the flame was elongated with the flowfield featuring an inner recirculation zone that extended throughout the optically accessibly field of view, namely with no downstream stagnation point. Upon approaching the transition, it was observed that the recirculation zone formed a downstream stagnation point and it initiated a precessing motion about the cylindrical centreline of the combustor. Subsequently, as the dynamic pressure rose towards its first peak, the recirculation zone, while still under precession, decreased in radial extent, while its downstream stagnation point was found at axial stations located increasingly closer to the inlet. The reason for the collapse of the recirculation zone was the convection, by the bulk flow, of an axial disturbance of enhanced heat release rate that decreased the swirl number. Close to requiescence, the recirculation zone recovered its previous open ended structure, with the precession decelerating with decreasing dynamic pressure amplitude. POD analysis of the transitional PIV flowfields revealed modes that have been typically associated in the literature with the existence of a Precessing Vortex Core structure. Analysis of the flame front curvature extracted via OH-PLIF images under an intermittent state of thermoacoustic operation was then pursued. The transitional flames were more wrinkled than their quiescent counterparts, as evidenced by the increased curvature standard deviations and the decreased corresponding kurtosis. Interestingly, examining the means and standard deviations of the spatial distribution of the turbulent intensity, it was observed that they both increase, on approaching the demonstration of a thermoacoustic burst. The latter observation corroborated the results of the OH-PLIF analysis with regards to the enhanced wrinkling of the flame. Nevertheless, it is not clear as to why intensified wrinkling and increased standard deviations of the turbulent intensity come about. Interpretation of these results are left as a subject of future investigation.

References

[1] Strutt, J. W., and Rayleigh, B., *The theory of sound*, Dover, 1945.

[2] Kabiraj, L., and Sujith, R., "Investigation of subcritical instability in ducted premixed flames," *ASME 2011 Turbo Expo: Turbine Technical Conference and Exposition*, American Society of Mechanical Engineers Digital Collection, 2011, pp. 969–977.

[3] Nair, V., Thampi, G., Karuppusamy, S., Gopalan, S., and Sujith, R. I., "Loss of chaos in combustion noise as a precursor of impending combustion instability," *International Journal of Spray and Combustion Dynamics*, Vol. 5, No. 4, 2013, pp. 273–290. doi:10.1260/1756-8277.5.4.273, URL http://www.scopus.com/inward/record.url?eid=2-s2.0-84885168482{&}partnerID=tZOtx3y1.

[4] Ebi, D., Denisov, A., Bonciolini, G., Boujo, E., and Noiray, N., "Flame Dynamics Intermittency in the Bistable Region Near a Subcritical Hopf Bifurcation," *Journal of Engineering for Gas Turbines and Power*, Vol. 140, No. 6, 2018, p. 061504.

[5] Nair, V., and Sujith, R. I., "Identifying homoclinic orbits in the dynamics of intermittent signals through recurrence quantification." *Chaos*, Vol. 23, No. 3, 2013, p. 033136. doi:10.1063/1.4821475, URL http://www.ncbi.nlm.nih.gov/pubmed/24089972.

[6] Kim, K. T., "Combustion instability feedback mechanisms in a lean-premixed swirl-stabilized combustor," *Combustion and Flame*, Vol. 171, 2016, pp. 137–151. doi:10.1016/j.combustflame.2016.06.003, URL http://dx.doi.org/10.1016/j.combustflame.2016.06.003.

[7] Kashinath, K., Waugh, I. C., and Juniper, M. P., "Nonlinear self-excited thermoacoustic oscillations of a ducted premixed flame: Bifurcations and routes to chaos," *Journal of Fluid Mechanics*, Vol. 761, 2014, pp. 399–430. doi:10.1017/jfm.2014.601.

[8] Dowling, A. P., and Mahmoudi, Y., "Combustion noise," *Proceedings of the Combustion Institute*, Vol. 35, No. 1, 2015, pp. 65–100. doi:10.1016/j.proci.2014.08.016, URL http://dx.doi.org/10.1016/j.proci.2014.08.016.

[9] Nair, V., and Sujith, R. I., "Intermittency as a Transition State in Combustor Dynamics: An Explanation for Flame Dynamics Near Lean Blowout," *Combustion Science and Technology*, Vol. 187, No. 11, 2015, pp. 1821–1835. doi:10.1080/00102202.2015.1066339, URL http://www.tandfonline.com/doi/full/10.1080/00102202.2015.1066339.

[10] Knoop, P., Culick, F., and Zukoski, E., "Extension of the stability of motions in a combustion chamber by nonlinear active control based on hysteresis," *Combustion science and technology*, Vol. 123, No. 1-6, 1997, pp. 363–376.

[11] Broda, J., Seo, S., Santoro, R., Shirhattikar, G., and Yang, V., "An experimental study of combustion dynamics of a premixed swirl injector," *Symposium (International) on Combustion*, Vol. 27, No. 2, 1998, pp. 1849–1856. doi:10.1016/S0082-0784(98)80027-1, URL http://www.sciencedirect.com/science/article/pii/S0082078498800271.

[12] Huang, Y., and Yang, V., "Bifurcation of flame structure in a lean-premixed swirl-stabilized combustor: transition from stable to unstable flame," *Combustion and Flame*, Vol. 136, No. 3, 2004, pp. 383–389. doi:10.1016/j.combustflame.2003.10.006, URL http://www.sciencedirect.com/science/article/pii/S0010218003002840.

[13] Lieuwen, T. C., "Experimental investigation of limit cycle oscillations in an unstable gas turbine combustor," *Journal of Propulsion and Power*, Vol. 18, No. 1, 2002, pp. 61–67.

[14] Nayfeh, A. H., and Balachandran, B., *Chapter 1: Introduction*, Vol. 104, 2009.

[15] Grassberger, P., and Procaccia, I., "Measuring the strangeness of strange attractors," *Physica D: Nonlinear Phenomena*, Vol. 9, No. 1-2, 1983, pp. 189–208. doi:10.1016/0167-2789(83)90298-1.

[16] Polifke, W., Fischer, A., and Sattelmayer, T., "Instability of a premix burner with nonmonotonic pressure drop characteristic," *Journal of engineering for gas turbines and power*, Vol. 125, No. 1, 2003, pp. 20–27.

[17] Moeck, J., Bothien, M., Schimek, S., Lacarelle, A., and Paschereit, C., "Subcritical thermoacoustic instabilities in a premixed combustor," *14th AIAA/CEAS aeroacoustics conference (29th AIAA aeroacoustics conference)*, 2008, p. 2946.

[18] Arndt, C. M., Steinberg, A. M., Boxx, I. G., Meier, W., Aigner, M., and Carter, C. D., "Flow-field and flame dynamics of a gas turbine model combustor during transition between thermo-acoustically stable and unstable states," *ASME Turbo Expo 2010: Power for Land, Sea, and Air*, American Society of Mechanical Engineers, 2010, pp. 677–687.

[19] Syred, N., "A review of oscillation mechanisms and the role of the precessing vortex core (PVC) in swirl combustion systems," *Progress in Energy and Combustion Science*, Vol. 32, No. 2, 2006, pp. 93–161. doi:10.1016/j.pecs.2005.10.002.

[20] Stöhr, M., Oberleithner, K., Sieber, M., Yin, Z., and Meier, W., "Experimental Study of Transient Mechanisms of Bistable Flame Shape Transitions in a Swirl Combustor," *Journal of Engineering for Gas Turbines and Power*, Vol. 140, No. 1, 2018, p. 011503.

[21] Taamallah, S., Shanbhogue, S. J., and Ghoniem, A. F., "Turbulent flame stabilization modes in premixed swirl combustion: Physical mechanism and Karlovitz number-based criterion," *Combustion and Flame*, Vol. 166, 2016, pp. 19–33. doi:10.1016/j.combustflame.2015.12.007, URL http://dx.doi.org/10.1016/j.combustflame.2015.12.007.

[22] Karlis, E., Liu, Y., Hardalupas, Y., and Taylor, A. M., "H2 enrichment of CH4 blends in lean premixed gas turbine combustion: An experimental study on effects on flame shape and thermoacoustic oscillation dynamics," *Fuel*, Vol. 254, 2019, p. 115524.

[23] Bandt, C., and Pompe, B., "Permutation entropy: a natural complexity measure for time series." *Physical review letters*, Vol. 88, No. 17, 2002, p. 174102. doi:10.1103/PhysRevLett.88.174102.

[24] Karlis, E., Liu, Y., Hardalupas, Y., and Taylor, A., "Extinction strain rate suppression of the precessing vortex core in a swirl stabilised combustor and consequences for thermoacoustic oscillations," *Combustion and Flame*, Vol. 211, No. 3, 2020, pp. 229–252. doi:10.1016/j.combustflame.2019.09.031.

[25] Lucca-Negro, O., and O'Doherty, T., "Vortex breakdown: A review," *Progress in Energy and Combustion Science*, Vol. 27, No. 4, 2001, pp. 431–481. doi:10.1016/S0360-1285(00)00022-8.

[26] Orain, M., and Hardalupas, Y., "Influence du combustible sur la mesure de richesse par chimiluminescence dans les flammes prémélangées," *Comptes Rendus - Mecanique*, Vol. 338, No. 5, 2010, pp. 241–254. doi:10.1016/j.crme.2010.05.002, URL http://dx.doi.org/10.1016/j.crme.2010.05.002.

[27] Panoutsos, C. S., Hardalupas, Y., and Taylor, A. M. K. P., "Effect of Preheating on the local Equivalence Ratio at a," *41st Aerospace Sciences Meeting and Exhibit, AIAA 2008-0960*, , No. January, 2008, pp. 1–13.

[28] Gaydon, A., *The spectroscopy of flames*, springer science & business media, 1974.

[29] Dieke, G., and Crosswhite, H., "The ultraviolet bands of OH fundamental data," *Journal of Quantitative Spectroscopy and Radiative Transfer*, Vol. 2, No. 2, 1962, pp. 97–199.

[30] Oberleithner, K., Stöhr, M., Im, S. H., Arndt, C. M., and Steinberg, A. M., "Formation and flame-induced suppression of the precessing vortex core in a swirl combustor: Experiments and linear stability analysis," *Combustion and Flame*, Vol. 162, No. 8, 2015, pp. 3100–3114. doi:10.1016/j.combustflame.2015.02.015, URL http://dx.doi.org/10.1016/j.combustflame.2015.02.015.

[31] Oberleithner, K., Schimek, S., and Paschereit, C. O., "Shear flow instabilities in swirl-stabilized combustors and their impact on the amplitude dependent flame response: A linear stability analysis," *Combustion and Flame*, Vol. 162, No. 1, 2015, pp. 86–99. doi:10.1016/j.combustflame.2014.07.012, URL http://dx.doi.org/10.1016/j.combustflame.2014.07.012.

[32] Moeck, J. P., Bourgouin, J. F., Durox, D., Schuller, T., and Candel, S., "Nonlinear interaction between a precessing vortex core and acoustic oscillations in a turbulent swirling flame," *Combustion and Flame*, Vol. 159, No. 8, 2012, pp. 2650–2668. doi:10.1016/j.combustflame.2012.04.002, URL http://dx.doi.org/10.1016/j.combustflame.2012.04.002.

[33] Stöhr, M., Boxx, I., Carter, C. D., and Meier, W., "Experimental study of vortex-flame interaction in a gas turbine model combustor," *Combustion and Flame*, Vol. 159, No. 8, 2012, pp. 2636–2649. doi:10.1016/j.combustflame.2012.03.020.

[34] Steinberg, A. M., Boxx, I., Stöhr, M., Carter, C. D., and Meier, W., "Flow-flame interactions causing acoustically coupled heat release fluctuations in a thermo-acoustically unstable gas turbine model combustor," *Combustion and Flame*, Vol. 157, No. 12, 2010, pp. 2250–2266. doi:10.1016/j.combustflame.2010.07.011, URL http://dx.doi.org/10.1016/j.combustflame.2010.07.011.

[35] Bayley, A. E., "Turbulent Flow Structure and Flame Characterisation of Lean Premixed Swirling Combustion," Ph.D. thesis, 2014.